Journal of Nuclear Materials 502 (2018) 68–75

Contents lists available at ScienceDirect

Journal of Nuclear Materials

journal homepage: www.elsevier.com/locate/jnucmat

Measurement of UO_2 surface oxidation using grazing-incidence x-ray diffraction: Implications for nuclear forensics

Cameron L. Tracy [a, b, *], Chien-Hung Chen [a], Sulgiye Park [a], M. Lee Davisson [c], Rodney C. Ewing [a, b]

[a] Department of Geological Sciences, Stanford University, Stanford, CA 94305, USA
[b] Center for International Security and Cooperation, Stanford University, Stanford, CA 94305, USA
[c] Physical and Life Sciences Directorate, Lawrence Livermore National Laboratory, Livermore, CA 94551, USA

HIGHLIGHTS

- UO_2 surfaces oxidize when exposed to air.
- Surface oxidation serves as a forensic signature of the handling of a sample.
- The extent of oxidation can be quantified using grazing-incidence x-ray diffraction.
- These measurements are sensitive to exposure temperature, but not to humidity.

ARTICLE INFO

Article history:
Received 4 October 2017
Received in revised form
19 December 2017
Accepted 28 January 2018
Available online 31 January 2018

Keywords:
UO_2
Oxidation
Grazing-incidence x-ray diffraction

ABSTRACT

Nuclear forensics involves determination of the origin and history of interdicted nuclear materials based on the detection of signatures associated with their production and trafficking. The surface oxidation undergone by UO_2 when exposed to air is a potential signature of its atmospheric exposure during handling and transport. To assess the sensitivity of this oxidation to atmospheric parameters, surface sensitive grazing-incidence x-ray diffraction (GIXRD) measurements were performed on UO_2 samples exposed to air of varying relative humidity (34%, 56%, and 95% RH) and temperature (room temperature, 50 °C, and 100 °C). Near-surface unit cell contraction was observed following exposure, indicating oxidation of the surface and accompanying reduction of the uranium cation ionic radii. The extent of unit cell contraction provides a measure of the extent of oxidation, allowing for comparison of the effects of various exposure conditions. No clear influence of relative humidity on the extent of oxidation was observed, with samples exhibiting similar degrees of unit cell contraction at all relative humidities investigated. In contrast, the thickness of the oxidized layers increased substantially with increasing temperature, such that differences on the order of 10 °C yielded readily observable crystallographic signatures of the exposure conditions.

1. Introduction

Nuclear power generation currently provides about 11% of the electricity consumed worldwide [1], relying primarily on the extraction of energy from UO_2 fuel, yet it also presents risks to international security. Some isotopes of uranium and the higher actinides into which it transmutes during reactor operation can be used to produce nuclear weapons. This makes nuclear fuel and related materials attractive targets for theft by those wishing to acquire these weapons, including non-state actors such as terrorist groups [2]. Following the collapse of the Soviet Union in 1991, which made vulnerable large quantities of nuclear materials, a new phenomenon of illicit nuclear smuggling emerged as a global security concern [3–5]. Several seizures of kilogram quantities of smuggled, weapons-usable nuclear materials have demonstrated the urgency of this threat [5].

While law enforcement and customs or border controls can aid in the interdiction of smuggled materials, advanced forensic techniques are needed to elucidate the origin of the material, or its

* Corresponding author. Department of Geological Sciences, Stanford University, Stanford, CA 94305, USA.
E-mail address: cltracy@stanford.edu (C.L. Tracy).

https://doi.org/10.1016/j.jnucmat.2018.01.052
0022-3115/

provenance, and the means by which it was smuggled to the point of interdiction. Nuclear forensics relies mainly on the use of analytical techniques to characterize physical or chemical "signatures" associated with the history of an interdicted sample [2–4,6,7]. For example, analyses of chemical and isotopic composition can reveal information about where the uranium in a sample was mined. Likewise, measurement of physical characteristics like grain size can be used to determine the factory at which a fuel pellet was manufactured. However, it is much more difficult to ascertain the specific means and route by which a sample was smuggled, as the illicit storage and transport of materials typically have little or no effect on properties like isotopic composition and grain size. Thus, there is a widely-acknowledged need for the identification of new, potentially useful signatures associated with the means by which nuclear materials were stored or transported after their theft [2,4,6].

One promising source of such signatures for UO_2 is the oxidation it undergoes during exposure to air. Even below room temperature, UO_2 will slowly oxidize to a hyperstoichiometric compound, UO_{2+x}, and eventually to more oxygen-rich compounds such as U_4O_9, U_3O_7, and U_3O_8 [8–11]. Near room temperature, the sluggish diffusion of oxygen in UO_2 yields slow penetration from the solid/air interface, such that oxidation is confined to a thin, near-surface layer terminating at an oxidation front [9,12]. Typically, at near room temperature conditions only the initial stages of adventitious oxygen incorporation into the fluorite structure (space group *Fm*-3*m*) of UO_2 occur. This yields either UO_{2+x} or U_4O_9, which adopts structures similar to that of UO_2, with additional oxygen anions arranged in cuboctahedral clusters [13]. The formation of U_3O_7 or higher oxides has not been reported above ~150 °C [12]. Analysis of this oxidized layer and its thickness could provide useful information on the atmospheric conditions to which a UO_2 sample was exposed, assuming atmospheric parameters influence the penetration of oxygen into the sample surface. In other words, surface oxidation could serve as a forensic signature yielding information related to the manner in which a trafficked sample was stored or transported. This approach is analogous to the well-developed obsidian hydration dating (OHD) technique used in archaeology, wherein the thickness of the hydration rinds present on obsidian artifacts are related to their ages by considering the diffusion rate of water into the obsidian surface [14].

As the extent of oxygen diffusion is time dependent, the extent of surface oxidation likely corresponds to the time for which a sample was exposed to atmosphere. Furthermore, the diffusivity of oxygen in UO_2 is temperature dependent [15], such that the thickness of the oxidized layer might be used to constrain the temperature conditions in which a smuggled UO_2 sample was stored or transported. In addition to temperature, the relative humidity of the atmosphere to which UO_2 is exposed may affect its oxidation. Numerous density functional theory (DFT) calculations [16–23] predict that water will adsorb dissociatively on steps or defects on the UO_2 surface, which has been confirmed experimentally [24–28]. However, the manner in which the adsorbed species influence the penetration of oxygen below the surface remains largely unexplored. Although the relevant experimental data are sparse and sometimes contradictory, they do suggest that humidity slightly enhances oxidation, yet most experiments were carried out at temperatures above ~150 °C [12]. These high temperatures are commonly studied because they reflect the extreme conditions experienced by nuclear fuel in a reactor and spent fuel in storage [29], but they are of limited relevance to the smuggling of UO_2.

For nuclear forensics applications, the thickness of the oxidized surface layer of UO_2 would ideally be characterized using a relatively common, readily available experimental method. To this end, grazing-incidence x-ray diffraction (GIXRD) was investigated as a means of characterizing the unit cell contraction that accompanies surface oxidation [30,31], due to the smaller ionic radius of U^{6+} (0.86 Å in eightfold coordination) relative to U^{4+} (1.00 Å in eightfold coordination) [32]. GIXRD is a common, well-established crystallographic technique that can be performed at the laboratory scale. X-ray diffraction measurements are commonly used to assess the oxygen content of UO_{2+x} [31,33], and grazing-incidence geometry provides surface sensitivity. At room temperature, no observable effect of humidity on the oxidized layer thickness could be ascertained. However, a clear influence of temperature was observed, even between exposures at room temperature and 50 °C. These results show that the oxidized layer thickness could serve as a useful forensic signature for the analysis of interdicted UO_2 and that it can be characterized using relatively common techniques.

2. Experimental methods

Stoichiometric UO_2 reference samples of natural isotopic composition were obtained from New Brunswick Laboratory, the United States Government's provider of nuclear reference materials. These samples, in the form of 1 cm diameter pellets, were sliced into disks, polished with diamond paste to a grade of 1 μm, and cut into quarters. All samples were sealed in an inert atmosphere prior to controlled exposure to air.

The UO_2 samples were exposed for 39 days to room temperature air (20% O_2) with relative humidities (RH) of 34%, 56%, and 95%. The relative humidity was controlled by the addition of inorganic salt slurries to the exposure chambers: $CaCl_2{\bullet}6H_2O$, $Mg(NO_3)_2{\bullet}6H_2O$, and K_2SO_4, respectively, to achieve the three relative humidities used. Humidity was monitored using a hygrometer. Additional samples were exposed to air at 95% RH within a tube furnace at temperatures of 50 °C and 100 °C for 10 days. A control sample was not exposed to air after preparation, and was instead stored in a nitrogen purged glovebox in order to prevent oxidation of the surface.

After exposure, each sample was sealed in two layers of Kapton tape to facilitate handling of the radioactive material and to reduce atmospheric exposure during GIXRD characterization. GIXRD measurements were performed at beamline A2 of the Cornell High Energy Synchrotron Source (CHESS), which is equipped with a 4-circle goniometer for precise control of the x-ray incident angle, ω (see Fig. 1). An x-ray wavelength of 1.0221 Å was used, with a beam size of 0.5 mm in the vertical direction and 1 cm in the horizontal direction. Diffraction patterns were measured over the 2θ range 16–46°, with a total collection time of 360 s for each pattern.

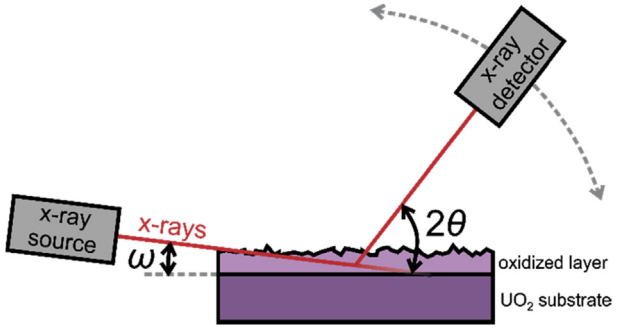

Fig. 1. A schematic illustration of a GIXRD measurement of an oxidized UO_2 pellet. During data collection, the x-ray incident angle ω is fixed while the point detector rotates over the desired 2θ measurement range. By varying ω the penetration of x-rays into the sample surface can be controlled, such that information on the thickness of the oxidized layer can be extracted.

This range includes six peaks of the typical fluorite structure of UO_2, including the four most intense, making it suitable for structure determination and analysis while also allowing for the adequate signal to be maintained using reasonable collection times.

GIXRD geometry was used to reduce the relatively large penetration depths that are typical of x-rays, which make conventional $\theta/2\theta$ methods insensitive to the sample surface. GIXRD makes use of a shallow incident x-ray angle to minimize the depth into the sample surface that is probed by the beam [34], as illustrated in Fig. 1. This asymmetric Bragg geometry can be varied to obtain a quantitative depth profile of the atomic structure [35]. However, below a certain critical angle, θ_c, which is x-ray wavelength and material dependent, total external reflection of the x-rays will occur [36]. This critical angle is equal to $\sqrt{2\delta}$, where δ is the real component of the refractive index, given by:

$$\delta = \frac{n_a r_e \lambda^2 f_1}{2\pi} \tag{1}$$

where n_a is the atomic number density, r_e is the classical electron radius, λ is the x-ray wavelength, and f_1 is the dispersive atomic scattering factor. Equation (1) yields a critical angle of $\theta_c = 0.28^\circ$ for 1.0221 Å x-rays in UO_2. Therefore, GIXRD measurements were performed at incident angles in the range $\omega = 0.3–12^\circ$.

As the incident angle is varied, both the refraction of x-rays at the sample surface and the absorption of x-rays within the sample change. Thus, increasing the incident angle increases the x-ray penetration depth, Λ, according to the expression [34,36]:

$$\Lambda = \frac{\lambda}{4\pi(B_i + B_e)} \tag{2}$$

where B_i and B_e are given by:

$$B_{i,e} = \frac{1}{\sqrt{2}}\left(\sqrt{\left(\theta_{i,e}^2 - \theta_c^2\right)^2 + 4\beta^2} + \theta_c^2 - \theta_{i,e}^2\right)^{1/2} \tag{3}$$

where θ_i is the incident angle relative to the sample surface, θ_e is the angle of the diffracted photons relative to the sample surface, and β is the imaginary component of the refractive index. This imaginary component is equal to:

$$\beta = \frac{n_a r_e \lambda^2 f_2}{2\pi} \tag{4}$$

where f_2 is the absorptive component of the atomic scattering factor. As seen from Equation (3), the x-ray penetration depth also varies with the angle of the diffracted photons relative to the sample surface, such that the sample depth probed varies with 2θ, when the incident beam angle is held constant. This is caused by the effects of the x-ray path geometry on the refraction of x-rays at the sample surface and the absorption of x-rays within the sample, as illustrated in Fig. 1. Due to the resulting proportionality of scattering depth with 2θ, each peak in a collected diffraction pattern corresponds to a slightly different probed sample depth.

The penetration depths of 1.0221 Å x-rays in UO_2, calculated using Equation (2), are shown in Fig. 2 as a function of incident angle for the (111) and (400) diffraction maxima. These peaks have the lowest and highest 2θ positions within the range measured, and therefore have the lowest and highest penetration depths, respectively. By varying the x-ray incident angle, a wide range of scattering depths was achieved. Some error in the precise depth probed at a given incident angle results from surface roughness that unavoidably forms during the oxidation process.

Prior to analysis of the diffraction patterns, corrections were applied to the 2θ positions of each measured data point to account for the effects of x-ray refraction at the sample surface, which causes small shifts in the observed diffraction angles [37]. The correction, $\Delta 2\theta$, that was applied to each data point is given by the formula:

$$\Delta 2\theta = \delta[\cot\omega + \cot(2\theta - \omega) + 2\tan\theta] \tag{5}$$

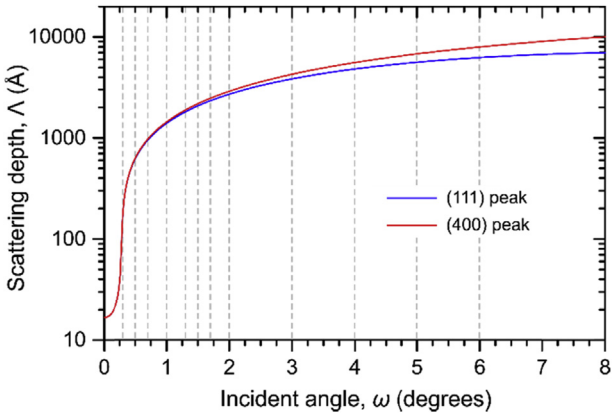

Fig. 2. The scattering depth, Λ, from which diffraction data was collected as a function of the x-ray incident angle, as calculated using Eq. (2) for two diffraction peaks, (111) and (400). The x-ray incident angles used in this work are denoted by vertical dashed lines. They provide data corresponding to a wide range of scattering depths.

The use of synchrotron radiation, rather than a laboratory x-ray source, proved advantageous in this analysis because it allowed for the use of a low x-ray wavelength. This wavelength is proportional to θ_c, Λ, and $\Delta 2\theta$.

Following GIXRD characterization and correction of the measured data, diffraction peak positions were analyzed by fitting of the (111) peaks with pseudo-Voigt profiles. Total pattern refinement was not performed because the x-ray penetration depth varies with 2θ (see Fig. 2), such that each peak corresponds to a different penetration depth. Thus, in this instance, total pattern fitting yields inferior depth resolution, because it involves convolution of data representing differing sample depths. In effect, if the unit cell parameter of a sample varies with depth, each diffraction peak will yield a distinct unit cell parameter. To address this problem, and to maximize the depth resolution achieved, this portion of the analysis was restricted to the (111) peak, which has the lowest corresponding x-ray penetration depth. Bragg's law was used to convert the fitted peak positions to unit cell parameters, *a*. The variance in the unit cell parameters as a function of x-ray penetration depth was studied in order to determine the extent to which the oxidized layer, which exhibits a smaller unit cell parameter than does the unoxidized substrate, contributes to the signal at a specific x-ray incident angle. The relative contribution of the oxidized layer at a specific scattering depth is proportional to the thickness of the layer, and thus to the extent of surface oxidation.

3. Results and discussion

3.1. Oxidation-induced modification of the GIXRD patterns

After exposure to air, diffraction patterns collected from all samples were checked for the appearance of new maxima that would indicate the appearance of non-cubic oxidation products such as U_3O_7 or U_3O_8. No new peaks were apparent in any of the patterns. Rather, all samples exhibited patterns similar to those of

ideal fluorite-structured UO_2 at all incident x-ray angles. This suggests that the oxidation product in the near-surface region is either UO_{2+x} or U_4O_9, both of which possess fluorite-like cation sublattices with adventitious oxygen incorporated in interstitial sites. Because x-ray scattering is dominated by the contributions of the heavy cations, this adventitious oxygen has little effect on the diffraction patterns, other than its indirect role in unit cell contraction that accompanies the increase in cation oxidation state needed to maintain charge balance. This result is consistent with previous XRD studies showing no formation of non-cubic higher oxides at temperatures below 100 °C [38].

Fig. 3 shows representative patterns, at a range of incident angles, obtained from the sample exposed to air of 95% RH at room temperature. The most obvious effects of increasing incident angle (increasing x-ray penetration depth, see Fig. 2) are an increase in peak intensity and a decrease in peak breadth. These effects are consistent with the presence of heterogeneous microstrain near the surface, resulting from surface stresses, which yield peak broadening [39]. Analysis of individual diffraction maxima reveals more substantial modifications as a function of x-ray incident angle. Fig. 4 shows representative GIXRD data, with the (111) peaks magnified, of samples exposed to air of 95% RH at room temperature and at 100 °C. Patterns obtained from both samples show shifts of the diffraction maxima to higher 2θ angles, corresponding to smaller unit cell parameters, as the x-ray incident angles are decreased. This is indicative of a contraction of the unit cell near the sample surface, caused by the oxidation of uranium and the concomitant reduction of its average ionic radius. This radius contraction results from the decreased shielding experienced by each electron on a uranium atom as electrons are removed during the oxidation process, such that the remaining electrons are more strongly drawn towards the nucleus [40].

The work of Stubbs et al. [41] has shown that the surface oxidation of UO_2 in air at room temperature proceeds by a

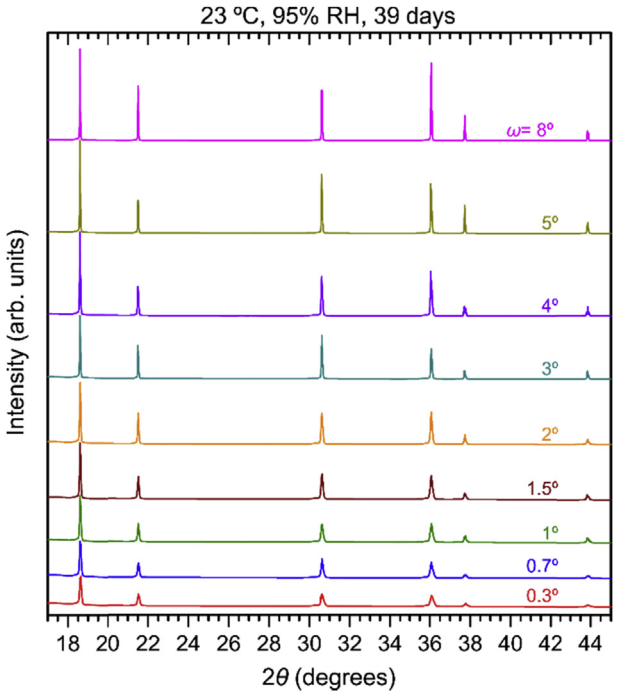

Fig. 3. GIXRD patterns obtained from UO_2 exposed to air at 95% RH and room temperature for 39 days, collected at various x-ray incident angles. With increasing incident angle, ω, the diffraction maxima become less broad and more intense. All peaks can be indexed to a fluorite-like atomic structure.

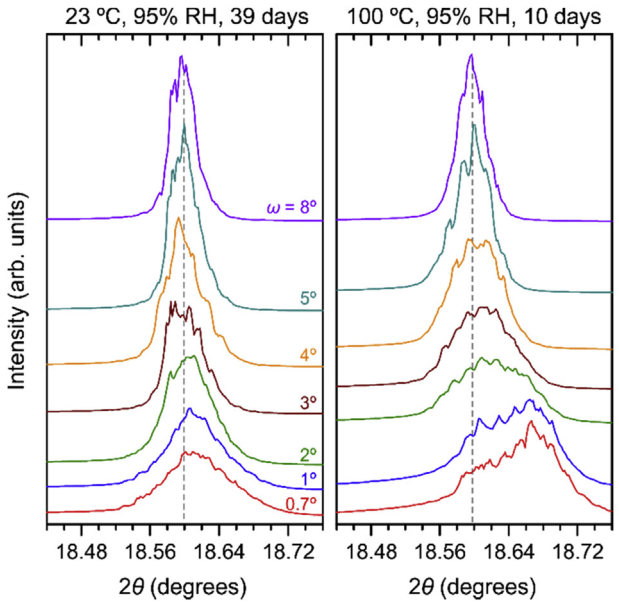

Fig. 4. A selected region of GIXRD patterns obtained from UO_2 exposed to air at 95% RH and room temperature for 39 days (left) and air at 95% RH and 100 °C for 10 days (right). Small peaks shifts are observed as the x-ray incident angle, ω, is varied. The low incident angle peaks of the sample exposed at high temperature show clear peak splitting, indicating that the signal arises from two overlapping peaks possessing different unit cell parameters. This unit cell parameter change at low incident angles is consistent with the oxidation of a thin surface layer. The clear difference in the relative intensities of the two peaks as a function of exposure condition suggests a strong influence of temperature on the extent of surface oxidation.

nonclassical diffusion mechanism that yields discrete, well delineated, nearly homogeneous layers of oxidized material atop an unoxidized UO_2 substrate. This agrees with prior work reporting the presence of discrete oxidized layers that slowly penetrate UO_2 surfaces along an oxidation front [12]. Assuming that this behavior holds true under the exposure conditions used in this work, the peak shifts observed here result from the superposition of two peaks: one with a relatively small unit cell parameter, arising from the thin, oxidized surface layer, and another with a relatively large unit cell parameter, arising from the unoxidized substrate. This interpretation is supported by the splitting of two distinct, overlapping peaks exhibited by the low x-ray incident angle pattern of the sample exposed at 100 °C. In the other patterns, the higher 2θ peak is too weak for unambiguous deconvolution of the two peaks, but clear asymmetry can be seen on the high 2θ side of the combined peak envelope, corroborating this interpretation.

While these two peaks cannot be reliably deconvoluted, a semi-quantitative determination of the relative contributions of each peak to each pattern can be performed by fitting of the combined peak envelope with a single pseudo-Voigt profile. This yields a single 2θ position of the fitted peak profile that varies with the relative contribution of each peak (high and low 2θ) to the pattern. As the x-ray incident angle increases, so too does the depth below the surface that is probed (see Fig. 2). Thus, with increasing ω more of the unoxidized substrate will be probed, and the relative contribution of the oxidized surface layer to the collected signal will decrease. The rate of this decrease, as a function of incident angle, will vary with the thickness of the oxidized layer, such that the experiments performed here provide information on the extent of oxidation, defined as the depth to which the oxidation front has penetrated during the air exposure period.

The minimum x-ray penetration depth achieved in these experiments, at an x-ray incident angle of $\omega = 0.3°$, is $\Lambda = 174$ Å (see

Fig. 2). In the experiments of Stubbs et al. [41] an oxidized layer of ~35 Å thickness was produced by exposure to dry air for 21 days. Barring an extreme influence of temperature or relative humidity on the oxygen penetration rate, oxidized layer thicknesses greater than the minimum x-ray penetration depth achieved in the experiments reported here are not expected. Thus, it can be assumed that all patterns measured here, and therefore all unit cell parameters reported, represent a weighted average of contributions from both the oxidized surface layer and the unoxidized substrate. At a sufficiently high x-ray incident angle, the contribution of the thin oxidized layer will become negligible relative to that of the substrate, and the unit cell parameter value extracted from peak fitting of these patterns should reach the typical value for stoichiometric UO_2.

3.2. The effects of relative humidity

To assess the effects of relative humidity on the surface oxidation of UO_2, as well as the sensitivity of GIXRD to any such effects, the measured unit cell parameters as a function of x-ray incident angle were compared among the three samples exposed to moist air at room temperature for 39 days, as well as the unexposed control sample. Fig. 5 shows the data corresponding to these four samples. At high x-ray incident angles, for which the relative contribution of the oxidized surface layer to the GIXRD patterns is assumed to be negligible, the measured unit cell parameters of all samples are approximately 5.4718 Å, in reasonable agreement with the literature value of 5.4713 Å for stoichiometric UO_2 [42]. In agreement with the trend shown in Fig. 4, the measured unit cell parameters decrease as the incident angle is reduced, indicating increasing contributions from the oxidized layer. This near-surface unit cell contraction is small for the unexposed control sample, indicating that it has undergone minimal surface oxidation. The small decrease observed at low x-ray incident angles likely arises from oxidation that occurred during the GIXRD measurements, which were performed in air.

In contrast, the samples exposed to air for 39 days show a much larger contraction of the unit cell at small incident angles. This indicates the presence of a thicker oxidized surface layer, which contributes more significantly to the GIXRD signal at a given x-ray incident angle. The lack of saturation of the unit cell parameter at the smallest x-ray incident angles suggests that the oxidized layer is thin relative to even the shallowest x-ray penetration depths achieved ($\Lambda = 174$ Å), consistent with the low average oxygen penetration rates (<2 Å/day) measured by Stubbs et al. [41] under similar conditions. Comparing the variation in unit cell parameter, as a function of x-ray incident angle, among the various exposure conditions reveals no observable effect of relative humidity on the extent of surface oxidation. This suggests that, at this temperature, either relative humidity does not have a substantial effect on the surface oxidation of UO_2, or that its effect is small enough that the resolution of the GIXRD measurements is insufficient for its observation.

Previous experiments suggest that the oxygen formed during the dissociation of gaseous water on the surface of UO_2 can proceed to penetrate the surface of the solid, facilitating surface oxidation [24]. However, it is unclear whether this process enhances oxidation in moist air, as oxygen is already available in the form of gaseous O_2. DFT calculations have predicted that the presence of water on the UO_2 surface enhances the adsorption of atmospheric oxygen onto the surface [19], yet insensitivity of the oxygen penetration rate to atmospheric humidity is still possible if it is the slow diffusion of oxygen into the solid, rather than its adsorption onto the surface, that acts as the rate limiting step of oxidized layer growth. Analysis of the variation in oxidized layer thickness as a function of relative humidity using techniques more sensitive than the GIXRD methods used here might further clarify the role of humidity in the surface oxidation of UO_2, but these more specialized techniques may be less conducive to the rapid characterization of interdicted samples in nuclear forensics applications. Additionally, the role of humidity in the surface oxidation of UO_2 may be more pronounced above room temperature, as the alteration products formed by exposure to water or water vapor at higher temperatures differ from those formed in dry air [43,44].

3.3. The effects of temperatures up to 100 °C

Unit cell parameters obtained from the samples exposed to air at 95% RH at temperatures of 50 °C and 100 °C for 10 days are shown in Fig. 6, alongside data obtained from the sample exposed to the same atmosphere at room temperature for 39 days. At high x-ray incident angles, the measured unit cell parameters of all samples are in reasonable agreement with the literature value for stoichiometric UO_2 [42]. As with the previously discussed samples, the

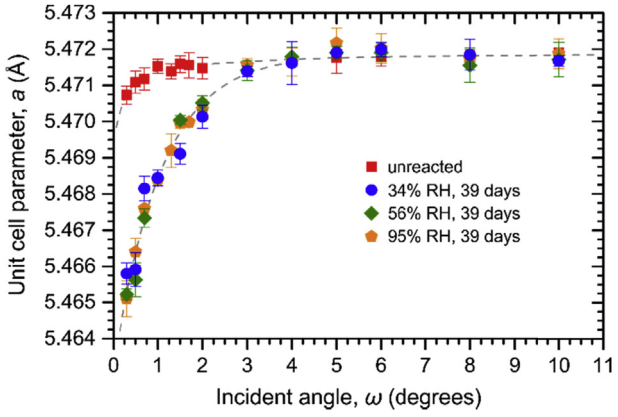

Fig. 5. Unit cell parameters, as a function of x-ray incident angle, determined by fitting of the (111) peaks of GIXRD patterns obtained from UO_2 samples. Data is shown for samples exposed for 39 days to room temperature air of varying relative humidity, as well as a control sample that was exposed only to an inert atmosphere. No clear influence of relative humidity on the extent of UO_2 surface oxidation is observed.

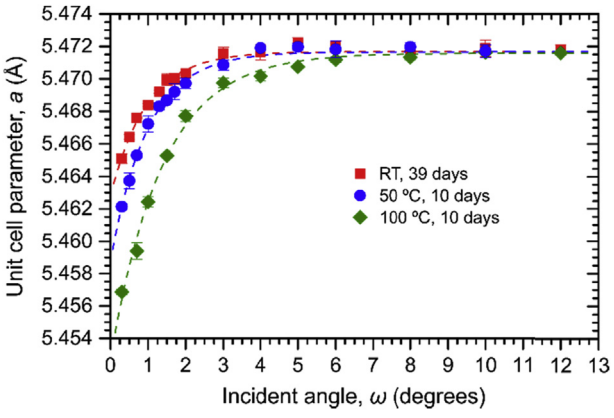

Fig. 6. Unit cell parameters, as a function of x-ray incident angle, determined by fitting of the (111) peaks of GIXRD patterns obtained from UO_2 samples. Data is shown for samples exposed for 10 days to air at 50 °C and 100 °C, as well as a sample that was exposed to air for 39 days at room temperature. Increasing temperature significantly enhances the near-surface unit cell contraction, indicating enhanced penetration of adventitious oxygen into the UO_2 surface and the formation of thicker oxidized surface layers.

measured unit cell parameter decreases with decreasing x-ray incident angle, indicating oxidation of a thin surface layer. However, the extent of this unit cell contraction is substantially increased for the samples exposed at temperatures greater than room temperature, particularly when accounting for the relatively short 10 day exposure time. These results indicate a strong influence of temperature on the surface oxidation rate, which is easily resolved by GIXRD measurements.

Most prior work has focused on the influence of temperatures above 150 °C on the oxidation of UO_2 [12]. However, the current results show that even small increases above room temperature, on the order of 10 °C, influence the surface oxidation in a manner readily observable using common GIXRD techniques. Specifically, the sample exposed at 50 °C for 10 days shows noticeably lower unit cell parameters, at low x-ray incident angles, than does the sample exposed at room temperature for 39 days, despite the fact that the former was exposed for only about one quarter the exposure time of the latter. This decreased unit cell parameter demonstrates a greater contribution of the oxidized layer to the signal arising from the x-ray penetration depth associated with low x-ray incident angles, which is indicative of a thicker oxidized layer resulting from thermally-enhanced oxygen diffusion into the surface. Even more extensive growth of the oxidized layer occurred at 100 °C. These results show that, in contrast to relative humidity, to which surface oxidation appears to be relatively insensitive, even small changes in temperature dramatically enhance the penetration of adventitious oxygen into the UO_2 surface. Thus, the extent of surface oxidation can serve as a forensic signature of the conditions under which a sample was exposed to air. Specifically, this sample parameter can be related quantitatively to the temperature at which exposure occurred and the period of time for which the sample was exposed.

Previous experimental work, reviewed by McEachern and Taylor [12], has shown that the diffusivity of oxygen in UO_2 is quite sensitive to temperature between room temperature and 100 °C. At temperatures up to roughly 50 °C, bulk oxygen diffusion is slow enough that oxidation is nearly always limited to a thin surface layer, yet as the temperature is increased above roughly 100 °C, bulk oxidation can occur following long exposure times [45–47]. This qualitative change in the character of the oxidation process suggests a significant thermal enhancement of diffusion-controlled surface oxidation over the temperature range studied, consistent with the findings reported here.

3.4. Complementary techniques

The GIXRD measurements of UO_2 surface oxidation demonstrated here provide information on the structural signatures of oxidation that is complementary to the chemical information provided by several spectroscopy techniques. For example, experiments on UO_2 exposed to air of varying relative humidity at room temperature have shown that x-ray photoelectron spectroscopy (XPS) is sensitive to the effects of humidity on oxidation state changes of near-surface uranium cations [48]. Thus, although no measureable influence of humidity on near-surface unit cell contraction was observed using GIXRD, XPS measurements could provide useful evidence of humidity exposure. These XPS measurements were performed using a method nearly identical to that used in the present work, confirming the conclusion drawn here that the observed unit cell expansion is related to an increase in the oxidation state of uranium. Similar near-surface oxidation state data has been obtained from UO_2 using laser-induced fluorescence spectroscopy [49].

Direct measurement of the oxidized layer thickness could also be obtained through electron microscopy imaging [50–52], but this can involve fairly extensive sample preparation. Similarly, secondary ion mass spectroscopy (SIMS) has been used for high resolution depth profiling of UO_2 oxygen content [53]. Finally, oxygen isotope analysis might provide useful information associated with the atmospheric exposure of interdicted samples, as isotopic composition varies with parameters such as geographic location [4,54–56].

4. Conclusions

GIXRD measurements of UO_2 exposed to air of varying relative humidity and temperature revealed near-surface unit cell contraction. This structural modification is attributed to the reduction of the uranium ionic radius accompanying the increase in its oxidation state that is required to maintain charge balance as adventitious oxygen penetrates the material surface. The extent of this unit cell contraction, and thus the extent of surface oxidation, showed little or no dependence on relative humidity, but a strong dependence on temperature. These results show that differences in the exposure temperature of a few tens of degrees Celsius, and possibly smaller, leave signatures that can be readily resolved via GIXRD measurements. A sample exposed at 50 °C for 10 days showed more extensive penetration of adventitious oxygen into the surface than did a sample exposed at room temperature for 39 days. Thus, an increase in temperature of ~20 °C roughly quadrupled the growth rate of the oxidized layer.

GIXRD characterization is a relatively straightforward technique that can be performed using laboratory-scale instruments, making it ideal for application to the nuclear forensics analysis of interdicted materials. These results demonstrate a potential application of this technique as a means to constrain the thermal conditions to which a smuggled UO_2 sample was exposed during trafficking. The potential utility of this information is illustrated by the two earliest instances of the theft of uranium-bearing materials following the fall of the Soviet Union, both of which involved long-term storage of the stolen material in an unheated environment [5]. In the first case the material was kept in the city of Podolsk, Russia, south of Moscow, while the second involved storage near Murmansk, Russia, north or the Arctic Circle. As the climates of these two locations differ substantially, variation in the extent of surface oxidation could have provided useful information, helping to constrain geographically the trafficking route of these materials had they been interdicted elsewhere.

One of the major limitations of the forensic method described here is the need for knowledge of the initial state of the sample, with respect to its surface condition. Thus, application of this method may be generally restricted only to pristine samples that have not undergone irradiation, as radiation damage and associated composition changes could introduce significant uncertainty to the initial state of the sample and might influence oxidation rate. Additionally, the requirement of a relatively large, flat surface limits the application of this method to pellets, excluding powder samples. Another important consideration is the similarity of the effects of exposure time and exposure temperature, both of which show proportionality with the extent of surface oxidation. Thus, it may not be possible to distinguish the effects of these two exposure parameters. For this reason, GIXRD analysis serves only to provide data helping to constrain the trafficking conditions experienced by an interdicted sample, rather than unambiguously determining them. This method would ideally be applied alongside a suite of complementary forensic techniques. Additionally, further study is needed to clarify the apparent insensitivity of surface oxygen penetration to relative humidity that was observed in this work, as this may arise from factors such as insufficient resolution of the experimental measurements.

Acknowledgements

The sample preparation and atmospheric exposure were funded by the Office of Defense Nuclear Nonproliferation, Research and Development within the U.S. Department of Energy's National Nuclear Security Administration under Project Number LL15-U_Surface Oxidation-NDD3B. This work was performed under the auspices of the U.S. Department of Energy by Lawrence Livermore National Laboratory under Contract DE-AC52-07NA27344. The collection and analysis of the diffraction data by CLT, CHC, and RCE were partially supported by the Energy Frontier Research Center "Materials Science of Actinides" funded by the U.S. Department of Energy (DOE), Office of Science, Office of Basic Energy Sciences (Grant No. DE-SC0001089). This work is based upon research conducted at the Cornell High Energy Synchrotron Source (CHESS) which is supported by the National Science Foundation under award DMR-1332208.

References

[1] Technology Roadmap: Nuclear Energy: 2015 Edition, International Energy Agency and Nuclear Energy Agency, 2015.
[2] K. Mayer, Expand nuclear forensics, Nature 503 (2013) 461–462, https://doi.org/10.1038/503461a.
[3] K. Mayer, M. Wallenius, T. Fanghänel, Nuclear forensic science—from cradle to maturity, J. Alloy. Comp. 444–445 (2007) 50–56, https://doi.org/10.1016/j.jallcom.2007.01.164.
[4] K. Mayer, M. Wallenius, I. Ray, Nuclear forensics—a methodology providing clues on the origin of illicitly trafficked nuclear materials, Analyst 130 (2005) 433–441, https://doi.org/10.1039/b412922a.
[5] W.C. Potter, Before the deluge? Assessing the threat of nuclear leakage from the post-Soviet states, Arms Control Today 25 (1995) 9–16.
[6] E. Keegan, M.J. Kristo, M. Colella, M. Robel, R. Williams, R. Lindvall, et al., Nuclear forensic analysis of an unknown uranium ore concentrate sample seized in a criminal investigation in Australia, Forensic Sci. Int. 240 (2014) 111–121, https://doi.org/10.1016/j.forsciint.2014.04.004.
[7] T.L. Spano, A. Simonetti, E. Balboni, C. Dorais, P.C. Burns, Trace element and U isotope analysis of uraninite and ore concentrate: applications for nuclear forensic investigations, Appl. Geochem. 84 (2017) 277–285, https://doi.org/10.1016/j.apgeochem.2017.07.003.
[8] K.B. Alberman, J.S. Anderson, The oxides of uranium, J. Chem. Soc. (1947) S303–S311, https://doi.org/10.1039/JR949000S303.
[9] G. Rousseau, L. Desgranges, F. Charlot, N. Millot, J.C. Nièpce, M. Pijolat, et al., A detailed study of UO_2 to U_3O_8 oxidation phases and the associated rate-limiting steps, J. Nucl. Mater. 355 (2006) 10–20, https://doi.org/10.1016/j.jnucmat.2006.03.015.
[10] D.A. Andersson, G. Baldinozzi, L. Desgranges, D.R. Conradson, S.D. Conradson, Density functional theory calculations of UO_2 oxidation: evolution of UO_{2+x}, $U4O_{9-y}$, $U3O_7$, and $U3O_8$, Inorg. Chem. 52 (2013) 2769–2778, https://doi.org/10.1021/ic400118p.
[11] J. Janeczek, R.C. Ewing, L.E. Thomas, Oxidation of uraninite: does tetragonal U_3O_7 occur in nature? J. Nucl. Mater. 207 (1993) 177–191, https://doi.org/10.1016/0022-3115(93)90260-6.
[12] R.J. McEachern, P. Taylor, A review of the oxidation of uranium dioxide at temperatures below 400°C, J. Nucl. Mater. 254 (1998) 87–121, https://doi.org/10.1016/S0022-3115(97)00343-7.
[13] R.I. Cooper, B.T.M. Willis, Refinement of the structure of β-U_4O_9, Acta Crystallogr. A 60 (2004) 322–325, https://doi.org/10.1107/S010876730401219X.
[14] I. Liritzis, N. Laskaris, Fifty years of obsidian hydration dating in archaeology, J. Non-Cryst. Solids 357 (2011) 2011–2023, https://doi.org/10.1016/j.jnoncrysol.2011.02.048.
[15] B. Dorado, P. Garcia, G. Carlot, C. Davoisne, M. Fraczkiewicz, B. Pasquet, et al., First-principles calculation and experimental study of oxygen diffusion in uranium dioxide, Phys. Rev. B 83 (2011) 035126, https://doi.org/10.1103/PhysRevB.83.035126.
[16] P. Maldonado, L.Z. Evins, P.M. Oppeneer, Ab initio atomistic thermodynamics of water reacting with uranium dioxide Surfaces, J. Phys. Chem. C 118 (2014) 8491–8500, https://doi.org/10.1021/jp501715m.
[17] V. Alexandrov, T.Y. Shvareva, S. Hayun, M. Asta, A. Navrotsky, Actinide dioxides in water: interactions at the interface, J. Phys. Chem. Lett. 2 (2011) 3130–3134, https://doi.org/10.1021/jz201458x.
[18] X. Tian, H. Wang, H. Xiao, T. Gao, Adsorption of water on UO2(111) surface: density functional theory calculations, Comput. Mater. Sci. 91 (2014) 364–371, https://doi.org/10.1016/j.commatsci.2014.05.009.
[19] F.N. Skomurski, L.C. Shuller, R.C. Ewing, U. Becker, Corrosion of UO_2 and ThO_2: a quantum-mechanical investigation, J. Nucl. Mater. 375 (2008) 290–310, https://doi.org/10.1016/j.jnucmat.2007.12.007.
[20] T. Bo, J. Lan, Y. Zhao, Y. Zhang, C. He, Z. Chai, et al., First-principles study of water adsorption and dissociation on the UO_2 (111), (110) and (100) surfaces, J. Nucl. Mater. 454 (2014) 446–454, https://doi.org/10.1016/j.jnucmat.2014.09.001.
[21] T. Bo, J. Lan, C. Wang, Y. Zhao, C. He, Y. Zhang, et al., First-principles study of water reaction and H_2 formation on UO_2 (111) and (110) single crystal surfaces, J. Phys. Chem. C 118 (2014) 21935–21944, https://doi.org/10.1021/jp503614f.
[22] P.F. Weck, E. Kim, C.F. Jové-Colón, D.C. Sassani, On the role of strong electron correlations in the surface properties and chemistry of uranium dioxide, Dalton Trans. 42 (2013) 4570–4578, https://doi.org/10.1039/c3dt32536a.
[23] H. Idriss, Surface reactions of uranium oxide powder, thin films and single crystals, Surf. Sci. Rep. 65 (2010) 67–109, https://doi.org/10.1016/j.surfrep.2010.01.001.
[24] M.N. Hedhili, B.V. Yakshinskiy, T.E. Madey, Interaction of water vapor with UO_2(001), Surf. Sci. 445 (2000) 512–525, https://doi.org/10.1016/S0039-6028(99)01117-6.
[25] S.D. Senanayake, G.I.N. Waterhouse, A.S.Y. Chan, T.E. Madey, D.R. Mullins, H. Idriss, The reactions of water vapour on the surfaces of stoichiometric and reduced uranium dioxide: a high resolution XPS study, Catal. Today 120 (2007) 151–157, https://doi.org/10.1016/j.cattod.2006.07.040.
[26] J. Stultz, M.T. Paffett, S.A. Joyce, Thermal evolution of hydrogen following water adsorption on defective UO2 (100), J. Phys. Chem. B 108 (2004) 2362–2364, https://doi.org/10.1021/jp031066u.
[27] S. Cohen, M.H. Mintz, S. Zalkind, A. Seibert, T. Gouder, N. Shamir, Water chemisorption on a sputter deposited uranium dioxide film—Effect of defects, Solid State Ionics 263 (2014) 39–45, https://doi.org/10.1016/j.ssi.2014.05.003.
[28] S.D. Senanayake, H. Idriss, Water reactions over stoichiometric and reduced UO_2(111) single crystal surfaces, Surf. Sci. 563 (2004) 135–144, https://doi.org/10.1016/j.susc.2004.06.169.
[29] C.L. Tracy, M. Lang, F. Zhang, S. Park, R.I. Palomares, R.C. Ewing, Review of recent experimental results on the behavior of actinide-bearing oxides and related materials in extreme environments, Prog. Nucl. Energy 104 (2018) 342–358. https://doi.org/10.1016/j.pnucene.2016.09.012.
[30] A.M. Chaka, G.A.E. Oxford, J.E. Stubbs, P.J. Eng, J.R. Bargar, Density-functional theory investigation of oxidative corrosion of UO_2, Comput. Theor. Chem. 987 (2012) 90–102, https://doi.org/10.1016/j.comptc.2011.11.028.
[31] B.E. Schaner, Metallographic determination of the UO_2-U_4O_9 phase diagram, J. Nucl. Mater. 2 (1960) 110–120, https://doi.org/10.1016/0022-3115(60)90038-6.
[32] R. Shannon, Revised effective ionic radii and systematic studies of interatomic distances in halides and chalcogenides, Acta Crystallogr. A 32 (1976) 751–767, https://doi.org/10.1107/S0567739476001551.
[33] C.T. Walker, V.V. Rondinella, D. Papaioannou, S. Van Winckel, W. Goll, R. Manzel, On the oxidation state of UO_2 nuclear fuel at a burn-up of around 100 MWd/kgHM, J. Nucl. Mater. 345 (2005) 192–205, https://doi.org/10.1016/j.jnucmat.2005.05.010.
[34] G. Renaud, Oxide surfaces and metal/oxide interfaces studied by grazing incidence X-ray scattering, Surf. Sci. Rep. 32 (1998) 1–90, https://doi.org/10.1016/S0167-5729(98)00005-3.
[35] P. Colombi, P. Zanola, E. Bontempi, R. Roberti, M. Gelfi, L.E. Depero, Glancing-incidence X-ray diffraction for depth profiling of polycrystalline layers, J. Appl. Crystallogr. 39 (2006) 176–179, https://doi.org/10.1107/S0021889805042779.
[36] M.F. Toney, T.C. Huang, S. Brennan, Z. Rek, X-ray depth profiling of iron oxide thin films, J. Mater. Res. 3 (1988) 351–356, https://doi.org/10.1557/JMR.1988.0351.
[37] M. Hart, W. Parrish, M. Bellotto, G.S. Lim, The refractive-index correction in powder diffraction, Acta Crystallogr. A 44 (1988) 193–197, https://doi.org/10.1107/S010876738701050X.
[38] G. Leinders, J. Pakarinen, R. Delville, T. Cardinaels, K. Binnemans, M. Verwerft, Low-temperature oxidation of fine UO_2 powders: a process of nanosized domain development, Inorg. Chem. 55 (2016) 3915–3927, https://doi.org/10.1021/acs.inorgchem.6b00127.
[39] A.R. Stokes, A.J.C. Wilson, The diffraction of X rays by distorted crystal aggregates—I, Proc. Phys. Soc. 56 (1944), https://doi.org/10.1088/0959-5309/56/3/303.
[40] C.L. Tracy, M. Lang, J.M. Pray, F. Zhang, D. Popov, C. Park, et al., Redox response of actinide materials to highly-ionizing radiation, Nat. Commun. 6 (2015) 6133, https://doi.org/10.1038/ncomms7133.
[41] J.E. Stubbs, A.M. Chaka, E.S. Ilton, C.A. Biwer, M.H. Engelhard, J.R. Bargar, et al., UO_2 oxidative corrosion by nonclassical diffusion, Phys. Rev. Lett. 114 (2015) 246103, https://doi.org/10.1103/PhysRevLett.114.246103.
[42] G. Leinders, T. Cardinaels, K. Binnemans, M. Verwerft, Accurate lattice parameter measurements of stoichiometric uranium dioxide, J. Nucl. Mater. 459 (2015) 135–142, https://doi.org/10.1016/j.jnucmat.2015.01.029.
[43] R.J. Finch, E.C. Buck, P.A. Finn, J.K. Bates, Oxidative corrosion of spent UO_2 fuel in vapor and dripping groundwater at 90 °C, Mater. Res. Soc. Symp. Proc. 556 (1999) 431–438, https://doi.org/10.1557/PROC-556-431.
[44] D.J. Wronkiewicz, J.K. Bates, T.J. Gerding, E. Veleckis, B.S. Tani, Uranium release and secondary phase formation during unsaturated testing of UO_2 at 90°C, J. Nucl. Mater. 190 (1992) 107–127, https://doi.org/10.1016/0022-3115(92)90081-U.
[45] J.S. Anderson, L.E.J. Roberts, E.A. Harper, The oxides of Uranium. Part VII. The oxidation of uranium dioxide, J. Chem. Soc. (1955) 3946–3959, https://doi.org/10.1039/JR9550003946.
[46] P.E. Blackburn, J. Weissbart, E.A. Gulbransen, Oxidation of uranium dioxide,

J. Phys. Chem. 62 (1958) 902–908, https://doi.org/10.1021/j150566a002.
[47] D.E.Y. Walker, The oxidation of uranium dioxides, J. Appl. Chem. 15 (1965) 128–135, https://doi.org/10.1002/jctb.5010150304.
[48] S.B. Donald, Z.R. Dai, M.L. Davisson, J.R. Jeffries, A.J. Nelson, An XPS study on the impact of relative humidity on the aging of UO_2 powders, J. Nucl. Mater. 487 (2017) 105–112, https://doi.org/10.1016/j.jnucmat.2017.02.016.
[49] K. Grossmann, T. Arnold, R. Steudtner, S. Weiss, G. Bernhard, Visualizing different uranium oxidation states during the surface alteration of uraninite and uranium tetrachloride, Naturwissenschaften 96 (2009) 963–974, https://doi.org/10.1007/s00114-009-0558-1.
[50] A. Leenaers, L. Sannen, S. Van den Berghe, M. Verwerft, Oxidation of spent UO_2 fuel stored in moist environment, J. Nucl. Mater. 317 (2003) 226–233, https://doi.org/10.1016/S0022-3115(03)00104-1.
[51] L.E. Thomas, R.E. Einziger, Grain boundary oxidation of pressurized-water reactor spent fuel in air, Mater. Char. 28 (1992) 149–156, https://doi.org/10.1016/1044-5803(92)90038-J.
[52] L.E. Thomas, R.E. Einziger, R.E. Woodley, Microstructural examination of oxidized spent PWR fuel by transmission electron microscopy, J. Nucl. Mater. 166 (1989) 243–251, https://doi.org/10.1016/0022-3115(89)90221-3.
[53] I. Marchetti, F. Belloni, J. Himbert, P. Carbol, T. Fanghänel, Novel insights in the study of water penetration into polycrystalline UO_2 by secondary ion mass spectrometry, J. Nucl. Mater. 408 (2011) 54–60, https://doi.org/10.1016/j.jnucmat.2010.10.065.
[54] L. Pajo, G. Tamborini, G. Rasmussen, K. Mayer, L. Koch, A novel isotope analysis of oxygen in uranium oxides: comparison of secondary ion mass spectrometry, glow discharge mass spectrometry and thermal ionization mass spectrometry, Spectrochim. Acta, Part B 56 (2001) 541–549, https://doi.org/10.1016/S0584-8547(01)00219-1.
[55] L. Pajo, K. Mayer, L. Koch, Investigation of the oxygen isotopic composition in oxidic uranium compounds as a new property in nuclear forensic science, Fresenius' J. Anal. Chem. 371 (2001) 348–352, https://doi.org/10.1007/s002160100983.
[56] G. Tamborini, D. Phinney, O. Bildstein, M. Betti, Oxygen isotopic measurements by secondary ion mass spectrometry in uranium oxide microparticles: a nuclear forensic diagnostic, Anal. Chem. 74 (2002) 6098–6101, https://doi.org/10.1021/ac0259515.